01 Jan 2011

# Study Of Turbulence-radiation Interaction In Hypersonic Turbulent Boundary Layers

L. (Lian) Duan
*Missouri Unviersity of Science and Technology*, duanl@mst.edu

A. M. Feldick

M. P. Martín

M. F. Modest

*et. al. For a complete list of authors, see https://scholarsmine.mst.edu/mec_aereng_facwork/5452*



## Recommended Citation

L. Duan et al., "Study Of Turbulence-radiation Interaction In Hypersonic Turbulent Boundary Layers," *49th AIAA Aerospace Sciences Meeting Including the New Horizons Forum and Aerospace Exposition*, article no. AIAA-2011-749, American Institute of Aeronautics and Astronautics, Jan 2011.
The definitive version is available at https://doi.org/10.2514/6.2011-749

49th AIAA Aerospace Sciences Meeting including the New Horizons Forum and Aerospace Exposition
4 - 7 January 2011, Orlando, Florida

AIAA 2011-749

49th AIAA Aerospace Sciences Meeting, 4-7 January 2011, Orlando, Florida

# Study of Turbulence-Radiation Interaction in Hypersonic Turbulent Boundary layers

L. Duan*, A. M. Feldick†, M. P. Martín*, M. F. Modest+, D. A. Levin‡

*Department of Aerospace Engineering, University of Maryland, College Park, MD, 20742
†Department of Mechanical Engineering, Penn State University, University Park, PA 16802
+School of Engineering, University of California, Merced, CA 95344
‡Department of Aerospace Engineering, Penn State University, University Park, PA 16802



**In the paper, we conduct direct numerical simulations (DNS) to investigate the effect of turbulence-radiation interaction (TRI) in hypersonic turbulent boundary layers, representative of the Orion crew exploration vehicle (CEV) at peak heating condition during reentry. The radiative transfer equation (RTE) is solved using the tangent slab approximation.[1] The RTE solver is line-by-line (LBL) accurate, making use of a developed efficient spectral database[2] for spectral modeling. A multi-group full-spectrum correlated-k-distribution (FSCK) method[3] is used to reduce the number of RTE evaluations while preserving LBL accuracy. A nondimensional governing parameter to measure the significance of TRI is proposed, and the DNS fields with and without radiation coupling are used to assess TRI. Both the uncoupled and coupled results show that there is no sizable interaction between turbulence and radiation at the hypersonic environment under investigation. An explanation of why the intensity of TRI in the hypersonic boundary layer is smaller than that in many combustion flows is provided.**

## Nomenclature

| | |
|---|---|
| $\mathbf{q}_R$ | Radiative heat flux, W/m$^3$ |
| $\varepsilon$ | Total emission, W/m$^3$ |
| $A$ | Total absorption, W/m$^3$ |
| $n$ | Number density, m$^{-3}$ |
| $M$ | Mach number, dimensionless |
| $\rho$ | Density, kg/m$^3$ |
| $u$ | velocity, m/s |

| | |
|---|---|
| $T$ | Translational temperature, or temperature in general, K |
| $T_v$ | Vibrational temperature, K |
| $T_r$ | Rotational temperature, K |
| $T_e$ | Electron temperature, K |
| $p$ | pressure, $p = \sum_s \rho_s \frac{\hat{R}}{M_s} T$, Pa |
| $h$ | specific enthalpy, J/kg, or Planck's constant |
| $E$ | total energy, $E = \sum_s^{ns} \rho_s (e_s + \frac{1}{2} u_i u_i)$, J/m$^3$ |
| $\mu$ | mixture viscosity, kg/(m·s) |
| $S_{ij}$ | strain rate tensor, $S_{ij} = \frac{1}{2}(\partial u_i/\partial x_j + \partial u_j/\partial x_i)$, s$^{-1}$ |
| $\sigma_{ij}$ | shear stress tensor, $\sigma_{ij} = 2\mu S_{ij} - \frac{2}{3}\mu\delta_{ij} S_{kk}$, Pa |
| $\kappa$ | mixture thermal conductivity, J/(K·m·s) |
| $J$ | diffusive mass flux, kg/m$^2$·s |
| $\delta$ | Boundary layer thickness, m |
| $\theta$ | Momentum thickness, m |
| $\delta^*$ | Displacement thickness, m |
| $q$ | turbulence kinetic energy, $q = \frac{u'^2 + v'^2 + w'^2}{2}$, m$^2$/s$^2$ |
| $q_C$ | conductive heat flux, $q_{Cj} = -\kappa \frac{\partial T}{\partial x_j}$, J/(m$^2$·s) |
| $u_\tau$ | Friction velocity, m/s |
| $H$ | Shape factor, $H = \delta^*/\theta$, dimensionless |
| $Re_\theta$ | Reynolds number, $Re_\theta \equiv \frac{\rho_\delta u_\delta \theta}{\mu_\delta}$, dimensionless |
| $Re_{\delta 2}$ | Reynolds number, $Re_{\delta_2} \equiv \frac{\rho_\delta u_\delta \theta}{\mu_w}$, dimensionless |
| $Re_\tau$ | Reynolds number, $Re_\tau \equiv \frac{\rho_w u_\tau \delta}{\mu_w}$, dimensionless |
| $\epsilon$ | dissipation rate, m$^2$/s$^3$ |
| *Superscripts* | |
| $+$ | inner wall units |
| *Subscripts* | |
| $\delta$ | Boundary layer edge |
| $s$ | chemical species |

# I. Introduction

Thermal radiation has long been recognized to contribute significantly to the overall heat load[4] for spacecraft during entry into planetary atmospheres or Earth return, which typically has velocities exceeding 10km/s. The radiative heat load onto such vehicles comes from both the radiation within the boundary layer, as well as the transmission of external radiation hitting the boundary layer.

Most boundary layers on hypersonic vehicles are turbulent, and fluctuations in temperature and species composition cause fluctuations in the radiative source term $\nabla \cdot \mathbf{q}_R$. The nonlinear dependence of $\nabla \cdot \mathbf{q}_R$ on its parameters results in

$$\overline{\nabla \cdot \mathbf{q}_R(T, n_s)} \neq \nabla \cdot \mathbf{q}_R(\overline{T}, \overline{n}_s)$$

and the difference is referred to as TRI, where $\overline{(\cdot)}$ indicates a mean quantity.

TRI is a well-known phenomenon studied primarily in the combustion community. It is well recognized today that in the field of combustion TRI can lead to sharply increased radiative heat loads. See the reviews by Faeth et al.[5] and Modest,[6] for example. For hypersonic boundary layers, Duan et al.[7] conducted DNS tightly coupled with emission to assess emission TRI using conditions typical of Orion crew exploration vehicle (CEV) during re-entry. They used the optically-thin assumption to avoid modeling spectral dependencies and reduce the required computational time. They found that TRI due to local emission with the boundary layer only subtly increases total emission and has negligible influence on mean flow quantities (mean temperature, velocity) as well as turbulent kinetic energy, but significantly enhances the effect of reducing temperature fluctuations and total emission fluctuations. In addition, Feldick et al.[8] evaluated the effects of absorption TRI in the form of boundary layer absorption of radiation emitted in the shock layer using uncoupled DNS fields, and they found the effects of absorption TRI is minimal, although a slight decrease in boundary layer transmissivities is predicted.

A complete characterization of TRI in hypersonic boundary layers with a fully coupled spectrally accurate solution, taking into account the boundary layer absorption of radiation emitted both locally within boundary layer and in the shock-layer, has not yet been explored. In the current work, we will continue the study by Duan et al.[7] and Feldick et al.[8] and conduct DNS with radiation coupling including both emission and absorption to assess the effects of TRI in hypersonic turbulent boundary layers, using conditions typical of Orion crew exploration vehicle (CEV) during re-entry. The effects of TRI will be analyzed by first using an uncoupled DNS field, which neglects the backward influence of radiation on the flow, and then by using DNS with radiation coupled to the DNS solver.

The paper is structured as follows. The governing equations, constitutive and relations are introduced in Section II. The details of radiation modeling are introduced in Section III. The nondimensional governing parameter for estimating TRI is given in Section IV. Flow conditions for DNS are given in Section V. Numerical methods, and initial and boundary conditions, are given in Section VI. Results are given in Section VII. Finally, conclusions are given in Section VIII.

## II. Governing equations

The governing equations, constitutive relations and numerical method for simulation of chemically reacting flow are described in detail in Duan & Martín.[9] Therefore, only a cursory description is given here.

The equations describing the unsteady motion of a reacting fluid are given by the species mass, mass-averaged momentum, and total energy conservation equations, which, neglecting thermal non-equilibrium, are

$$\begin{aligned}
\frac{\partial \rho_s}{\partial t} + \frac{\partial}{\partial x_j}\Big(\rho_s u_j + J_{sj}\Big) &= w_s \\
\frac{\partial \rho u_i}{\partial t} + \frac{\partial}{\partial x_j}\Big(\rho u_i u_j + p\delta_{ij} - \sigma_{ij}\Big) &= 0 \\
\frac{\partial E}{\partial t} + \frac{\partial}{\partial x_j}\Big((E+p)u_j - u_i\sigma_{ij} + q_j + \sum_s J_{sj}h_s\Big) &= 0
\end{aligned} \tag{1}$$

When thermal radiation is included, the heat flux $q_j$ in the total energy equation is the sum of conductive heat flux $q_{Cj}$ and radiative heat flux $q_{Rj}$. The details of the calculation of the radiative heat flux is introduced in Section III.

The thermodynamic properties of high-temperature air species for evaluating total energy $E$ and internal energy $e_s$ are computed by NASA Lewis curve fits.[10] Mixture transport properties $\mu$ and $\kappa$ for evaluating stress tensor $\sigma_{ij}$ and conductive heat flux $q_{Cj}$ are calculated using the Gupta[11]-Yos[12] mixing rule. Fick's diffusion model with unity Lewis number is used for calculating species diffusion flux $J_{sj}$. An 11-species-air-reaction mechanism[13] is used for gas-phase reactions. The constitutive relations and chemical mechanism are consistent with those used by NASA in the DPLR code to compute Orion entry mean flow solutions.

## III. Radiation Modeling

The radiative transfer equation (RTE) will be solved by a one-dimensional tangent slab radiative solver.[1] During typical Earth reentry conditions, the diatomic species in the flow around the spacecraft may become highly dissociated and emission from the two atomic species N and O, including bound-bound, bound-free and free-free transitions, is the major source of radiation from the shock-layer. The atomic species are treated with the multi group Full Spectrum Correlated $k$-distribution of Bansal et al.,[14,15] taking advantage of the narrow-band $k$-distributions databases for N and O, which make on-the-fly full-spectrum $k$-distribution spectral properties more efficient.[16]

In the development of the FSCK method for atoms in nonequilibrium plasmas, Bansal et al. neglected the overlap between N and O species, which was found to be a valid assumption.[16,17] In contrast, overlap between atomic radiation and molecular bands may be important for some cases, particularly in the VUV part of the spectrum. Overlap between species is treated with a multi-scale $k$-distribution model[3] for gas mixtures in thermodynamic nonequilibrium. It was found that overlap between different species is not important in the wavelength range >1750 Å due to the optically thin nature of molecular bands. For this spectral range a gray model was applied for molecular bands and the full-spectrum $k$-distribution method was used to treat the atomic species. In the VUV region there is strong absorption by bands of $N_2$. In the $k$-distribution model the RTEs are solved separately for each emitting species and overlap with other species is treated in an approximate way. The spectral overlap between species is calculated such that the exact transmissivity of a homogeneous gas layer is recovered. This mixing model is coupled with the narrow-band $k$-distribution database and atomic continuum database to allow efficient determination of the overlap factor and solution of the RTE in nonequilibrium and nonhomogeneous gas mixtures following Bansal et al.[3]

## IV. Governing parameters for TRI

The difference between $\overline{\nabla \cdot \mathbf{q}_R(T, n_s)}$ and $\nabla \cdot \mathbf{q}_R(\overline{T}, \overline{n}_s)$ is a measure of TRI intensity and indicate how thermal radiation gets augmented due to turbulent fluctuation. In order to further predict how such augmentation effects influence the overall turbulence flow field, we propose the nondimensional parameters based on order-of-magnitude analysis.

Thermal radiation acts as a source/sink of energy in the total energy equation. The influence of thermal radiation on the turbulence flow field can be estimated by the radiative heat ratio $\overline{\Delta h}$ , defined as

$$\overline{\Delta h} \equiv \frac{\nabla \cdot \mathbf{q}_R(\overline{T}, \overline{n}_s)\tau_t}{\sum_{i=1}^{ns} \overline{\rho}_i \left(h_i(\overline{T}) + \frac{1}{2}\overline{u}_k\overline{u}_k\right)} \tag{2}$$

where $\tau_t$ is some characteristic turbulence time scale, the choice of which may be large-eddy turnover time

$\frac{\delta}{U_\delta}$, or $\frac{q}{\epsilon}$, which is the time scale for energy-containing eddies. $\overline{\Delta h}$ is the ratio of radiative heat gain/loss during the characteristic turbulence flow time to the total flow enthalpy, and provides a measure of the relative importance of thermal radiation to the overall turbulence flow field. If the magnitude of $\overline{\Delta h}$ is close to or larger than unity, a significant change in flow field by thermal radiation is expected.

By the same token, to estimate the enhanced heat gain/loss due to TRI, we introduce 'interaction' radiative heat ratio $\overline{\Delta h}^I$, which is defined as

$$\overline{\Delta h}^I \equiv \frac{\left(\overline{\nabla \cdot \mathbf{q}_R(T, n_s)} - \nabla \cdot \mathbf{q}_R(\overline{T}, \overline{n}_s)\right) \tau_t}{\sum_{i=1}^{ns} \overline{\rho}_i \left(h_i(\overline{T}) + \frac{1}{2}\overline{u}_k \overline{u}_k\right)} \tag{3}$$

where $\overline{\nabla \cdot \mathbf{q}(T, n_s)} - \nabla \cdot \mathbf{q}(\overline{T}, \overline{n}_s)$ is included to provide a measure for the intensity of TRI. The 'interaction' radiative heat ratio is the ratio of enhanced heat gain/loss due to TRI during the characteristic flow time to the total flow enthalpy, and provides a measure of the relative importance of TRI to the overall turbulence flow field. If the magnitude of $\overline{\Delta h}^I$ is close to or larger than unity, a significant change in flow field by TRI is expected.

## V. Flow conditions

We consider the boundary layer for Orion CEV, which enters the Earth's atmosphere at 9.5km/s, at an altitude of 53km, and angle of 18°. These conditions represent Earth entry, at peak heating. Table 1 shows the boundary layer edge conditions and wall parameters for the DNS domain, which are established by extracting them from a larger domain finite-volume RANS calculation. The RANS solution is obtained (as a courtesy from NASA Ames) using a well-established NASA CFD solver DPLR[18] and considers chemical reaction processes of 11 species: $N$, $O$, $N^+$, $O^+$, $N_2$, $O_2$, $NO$, $N_2^+$, $O_2^+$, $NO^+$ and $e$. Figure 1 shows the entire computational domain for the RANS finite-volume solution, and Figures 2($a$,$b$) show the identified DNS subdomain. The DNS subdomain lies toward the front of the craft, where the temperature and electron number density are high and radiation is strong, as shown in Figure 3. The temperatures as well as number densities of radiating species ($N$, $O$, $N_2^+$, $NO$, $O_2$ and $N_2$ for Earth reentry) along the line-of-sight are indicated in Figure 2($b$). For the presently estimated Orion peak heating conditions, it was found that the strong turbulence is limited to the aft region of the spacecraft, where radiation is weak. Therefore, to investigate a worst case scenario, a relatively large turbulence level (maximum $\sqrt{q}/u_\tau \approx 2.2$ or $\sqrt{q}/U_\delta \approx 7\%$), typical of that in the attached boundary layer aft region, is prescribed to the selected DNS subdomain. The analysis then represents a combination of strong turbulence together with strongest radiation to present a worst case scenario for an Earth entry of Orion, or of a hypothetical case of a larger vehicle, to determine whether or not TRI may be of importance. The use of one temperature model for the DNS subdomain is justified since the at the selected conditions the vibrational temperature is equal to the translational temperature throughout the boundary layer, as shown in Figure 3($a$).

## VI. Numerical method, initial and boundary conditions

Regarding the numerical method, the spatial derivatives are computed using a fourth-order accurate, bandwidth-optimized WENO scheme.[19] To perform the numerical integration, we use a third-order accurate low-storage Runge-Kutta method by Williamson.[20] The viscous terms are computed using a fourth-order

| $M_\delta$ | $\rho_\delta$(kg/m$^3$) | $T_\delta$(K) | $T_w$(K) | $Re_\theta$ | $Re_\tau$ | $Re_{\delta 2}$ | $\theta$(mm) | H | $\delta$(mm) |
|---|---|---|---|---|---|---|---|---|---|
| 0.153 | 0.011 | 9622 | 2607 | 73 | 314 | 214 | 4.0 | 0.1 | 23.5 |

**Table 1. Dimensional bounday layer edge and wall parameters for direct numerical simulations**



accurate central scheme. A description of the code and its validation are given are given in DNS mode in Martín[21] and Duan & Martín.[9]

The initial DNS flow field is obtained by first extracting the mean profiles from the RANS calculation at the location indicated in Figure 2, and then superimposing the fluctuating field. The fluctuating field is obtained by transforming that of an incompressible turbulent boundary layer DNS using well-established scaling laws. The details of this initialization technique are introduced by Martín.[21] The domain size ($L_x \times L_y \times L_z$), the grid size ($\Delta x \times \Delta y \times \Delta z$) and the number of grid points ($N_x \times N_y \times N_z$) for the initial DNS field are given in Table 2. We take the streamwise, spanwise, and wall-normal directions to be $x$, $y$, and $z$, respectively. Uniform grid spacings are used in the streamwise and spanwise directions with constant $\Delta x^+$ and $\Delta y^+$, where the superscript ($^+$) indicates scaling with inner, or wall values. Geometric stretching is used in the wall-normal direction, with $z_k = z_2(\alpha^{k-1} - 1)/(\alpha - 1)$.

| $L_x/\delta$ | $L_y/\delta$ | $L_z/\delta$ | $\Delta x^+$ | $\Delta y^+$ | $z_2^+$ | $\alpha$ | $N_x$ | $N_y$ | $N_z$ |
|---|---|---|---|---|---|---|---|---|---|
| 9.5 | 1.9 | 8.7 | 47.4 | 9.6 | 0.55 | 1.113 | 64 | 64 | 60 |

**Table 2. Grid resolution and domain size for the initial DNS field**

The sensitivity of the solution to the grid size can be assessed by grid-convergence study, as shown in Figure 4($a$-$b$), which plot the r.m.s velocity and temperature, respectively, with different number of grid points for the DNS case without radiation coupling. All the corresponding curves collapse to within 2%, indicating the insensitivity of the results to the grid sizes. Convergence studies have been conducted for all other DNS cases. It should be noticed that the resolution requirements for very cold wall simulations, as it is the case here, are not as stringent as those for simulations with adiabatic walls.[22]

Non-slip wall boundary conditions are used for the three velocity components. The wall temperature is prescribed and kept isothermal. An equilibrium catalytic boundary condition is used for species, i.e. species go to equilibrium state at the given wall temperature. Periodic boundary conditions have been used in the streamwise and spanwise directions.

Averages are computed over streamwise and spanwise directions for each field; then an ensemble average is calculated over fields spanning around one non-dimensional time unit. The time is non-dimensionalized by $\delta/u_\tau$. The average of $f$ over the $x-$ and $y-$directions will be denoted by $\bar{f}$, or $< f >$, and fluctuations about this mean will be denoted by $f'$.

# VII. Results

## A. DNS without radiation coupling

First, TRI is assessed using DNS fields without radiation coupling ($\nabla \cdot \mathbf{q} = 0$), which neglects the backward influence of radiation on the flow. The DNS is conducted with the same thermal and chemical models as the DPLR calculation and has similar mean temperature and species number densities (Figure 5) as the DPLR solution at the same location. Figure 6 plots normalized fluctuations in temperature and number densities across the boundary layer. It is shown that the maximum temperature fluctuation relative to the mean is about 9%, while the maximum fluctuations in species number densities range from 20% for $O$ to 60% for $O_2$.

To investigate how thermal radiation gets augmented due to turbulent fluctuations, Figure 7 plots $\overline{\nabla \cdot \mathbf{q}(T, n_s)}$ and $\nabla \cdot \mathbf{q}(\overline{T}, \overline{n}_s)$ across the boundary layer. It is shown that although the maximum relative difference between the 'turbulent' and 'laminar' radiative source terms may become large in regions where $\nabla \cdot \mathbf{q}(\overline{T}, \overline{n}_s)$ is small, the absolute difference remains small and is within $\pm 3$ W/cm$^3$ all through the boundary layer. The 'turbulent' and 'laminar' wall directed radiative heat fluxes $\overline{q_w(T, n_s)}$ and $q_w(\overline{T}, \overline{n}_s)$ are also similar with values 252.3W/cm$^2$ and 251.5W/cm$^2$, respectively.

To predict the effect of TRI on the turbulence flow field, Figure 8($a$) plots the 'interaction' radiative heat ratio (defined by Equation 3). It is shown that $\overline{\Delta h}^I$ is more than five orders of magnitude smaller than unity, indicating that the enhanced heat gain/loss due to TRI has little influence on the turbulence flow field.

The assessment of TRI using uncoupled DNS flow fields can be justified by Figure 8($b$), which shows that the radiative heat ratio $\overline{\Delta h}$ (defined by Equation 2) is also significantly smaller than unity, indicating minimal backward influence of radiation on the turbulence flow field.

## B. DNS with radiation coupling

We further study the influence of radiation on the turbulence flow field and TRI by performing DNS coupled with the RTE solver introduced in Section III.

Figure 9 shows that thermal radiation has negligible influences on both the mean temperature and temperature fluctuations. So is the mean and RMS of the radiative source term, as it is shown by Figure 10. The negligible difference between coupled and uncoupled results is consistent with the small value of $\overline{\Delta h}$.

The minimal influence of radiation on the turbulence flow field is different from the observations by Duan et al.,[7] who found significant reduction in both flow temperature and temperature fluctuations under similar flow conditions after only the emission is introduced (assuming $\nabla \cdot \mathbf{q} = \varepsilon$). In reality, however, the net radiative energy change for a given fluid element comes from both emission and absorption (i.e. $\nabla \cdot \mathbf{q} = \varepsilon + A$). For the current boundary layer flow, the thermal emission within the boundary layer is largely counterbalanced by the absorbed irradiation from the shock layer, as indicated by Figure 12, which shows that the magnitude of $\nabla \cdot \mathbf{q}$ is more than two orders of magnitude smaller than that of $\varepsilon$. As a result, the influence of overall thermal radiation on the turbulence flow field becomes much weaker.

The intensity of TRI is assessed using the coupled DNS flow field. Figure 11 shows the comparison between $\overline{\nabla \cdot \mathbf{q}(T, n_s))}$ and $\nabla \cdot \mathbf{q}(\overline{T}, \overline{n}_s)$. Similar to the uncoupled DNS results (Figure 7), small intensity of TRI is observed.

## VIII. Conclusions

We conducted direct numerical simulations of turbulent boundary layers to study turbulent-radiation interaction, using conditions typical of Orion crew exploration vehicle at peak heating during re-entry. DNS fields with and without radiation coupling are considered.

The uncoupled results show that turbulent fluctuations have only subtle influence on the radiative source term and wall directed radiative heat flux, and the couple results show that thermal radiation has minimal backward influence on overall turbulence flow field as well as TRI at the hypersonic environment under investigation. Both the uncoupled and coupled results show that the nondimensional governing parameters ($\overline{\Delta h}$ and $\overline{\Delta h^I}$) , which are derived based on the order-of-magnitude analysis, provide good metrics for estimating the influence of thermal radiation and TRI on the overall turbulence flow field.

The insignificant influence of TRI on the turbulent flow dynamics for hypersonic boundary layers is different from what have been found for many combustion flows, as described in Section I. The possible reason for the difference is that in typical Earth re-entry conditions, the atomic species such as $N$ and $O$ are the strongest radiators.[23] The generation of these radiating species requires the reaction of air, which happens at significantly higher temperatures ($T > 2500$K) than those for typical combustion applications. The significantly higher flow enthalpy required to initialize the air reactions overwhelms the enhanced heat gain/loss due to TRI, as indicated in Figure 8. However, given the limited number of flow conditions explored, further investigation may be necessary to confirm this argument.

## IX. Acknowledgments

This work is sponsored by NASA Constellation University Institutes Project (CUIP) Grant # NCC3-989. We thank Peter Gnoffo for insightful discussions, and the Space Technology Division in NASA Ames for providing for providing Reynolds-averaged Navier-Stokes solutions under flow conditions representative of crew exploration vehicles.

### References

[1]Feldick, A. M., Modest, M. F., and Levin, D. A., "Closely Coupled Flowfield-Radiation Interaction for Flowfields Created During Hypersonic Reentry," *AIAA Paper 2008-4104*, 2008.

[2]Sohn, I., Bansal, A., Levin, D. A., and Modest, M. F., "Advanced Radiation Calculations of Hypersonic Reentry Flows Using Efficient Databasing Schemes," *under consideration by Journal of Thermophysics and Heat Transfer, also AIAA Paper 2008-4019*, 2009.

[3]Bansal, A., Modest, M. F., and Levin, D. A., "k-Distributions for Gas Mixtures in Hypersonic Nonequilibrium Flows," *48th AIAA Aerospace Sciences Meeting, AIAA Paper 2010-234*, 2010.

[4]Whiting, E. E. and Park, C., "Radiative Heating at the Stagnation Point of the AFE Vehicle," Tech. rep., NASA Technical Memorandom 102829, 1990.

[5]Faeth, G. M., Gore, J. P., Chuech, S. G., and Jeng, S. M., "Radiation from Turbulent Diffusion Flames," *Annual Review of Numerical Fluid Mechanics and Heat Transfer*, Vol. 2, 1989, pp. 1–38.

[6]Modest, M. F., "Multiscale Modeling of Turbulence, Radiation and Combustion Interactions in Turbulent Flames," *International Journal of Multiscale Computational Engineering*, Vol. 3, No. 2, 2005, pp. 85–106.

[7]Duan, L., Martín, M. P., Sohn, I., Levin, D., and Modest, D., "Study of Emission Turbulence-radiation Interaction in Hypersonic Turbulent Boundary Layers," *accepted by AIAA Journal, also AIAA Paper 2010-0354*.

[8]Feldick, A., Duan, L., Modest, M., Martín, M., and Levin, D., "Influence of Interactions Between Turbulence and Radiation on Transmissivities in Hypersonic Turbulent Boundary Layers," *AIAA Paper No. 2010-1185*, 2010.

[9]Duan, L. and Martín, M. P., "An effective procedure for testing the validity of DNS of wall-bounded turbulence including finite-rate reactions," *AIAA Journal*, Vol. 47, No. 1, 2009, pp. 244–251.

[10]Gordon, S. and McBride, B., "Computer Program for Calculation of Complex Chemical Equilibrium Compositions and Applications," *NASA Reference Publication 1311*, 1994.

[11]Gupta, R., Yos, J., Thompson, R., and Lee, K., "A Review of Reaction Rates and Thermodynamic and Transport Properties for 11-Species Air Model for Chemical and Thermal Non-equilibrium Calculations to 30000$K$," *NASA RP-1232*, 1990.

[12]Yos, J., "Transport properties of nitrogen, hydrogen, oxygen, and air to 30,000 K," *Avco. Corp. Wilmington, MA, TR AD-TM-63-7*, 1963.

[13]Park, C., "Non-equilibrium Hypersonic Aerodynamics," *Wiley*, 1990.

[14]Bansal, A., Modest, M. F., and Levin, D. A., "Correlated-k Distribution Method for Atomic Radiation in Hypersonic Nonequilibrium flows," *47th AIAA Aerospace Sciences Conference, AIAA Paper 2009-1027*, 2009.

[15]Bansal, A., Modest, M. F., and Levin, D. A., "Narrow-band k-distribution Database for Atomic Radiation in Hypersonic Nonequilibrium Flows," *ASME Paper No. HT2009-88120*, 2009, ASME Summer Heat Transfer Conference.

[16]Bansal, A., Modest, M. F., and Levin, D. A., "Correlated-k Distribution Method for Atomic Radiation in Hypersonic Nonequilibrium flows," *Journal of Thermophysics and Heat Transfer*, 2009, accepted for publication.

[17]Bansal, A., Modest, M. F., and Levin, D. A., "Narrow-band k-distribution Database for Atomic Radiation in Hypersonic Nonequilibrium Flows," *Journal of Heat Transfer*, 2009, submitted for publication.

[18]Wright, M., "DPLR CFD code," *NASA Ames Research Center, Moffett Field CA*.

[19]Taylor, E. M., Wu, M., and Martín, M. P., "Optimization of Nonlinear Error Sources for Weighted Non-Oscillatory Methods in Direct Numerical Simulations of Compressible Turbulence," *Journal of Computational Physics*, Vol. 223, 2007, pp. 384–397.

[20]Williamson, J. H., "Low-storage Runge-Kutta Schemes," *Journal of Computational Physics*, Vol. 35(1), 1980, pp. 48–56.

[21]Martín, M. P., "DNS of Hypersonic Turbulent Boundary Layers. Part I: Initialization and Comparison with Experiments," *Journal of Fluid Mechanics*, Vol. 570, 2007, pp. 347–364.

[22]Duan, L., Beekman, I., and Martín, M. P., "Direct numerical simulation of hypersonic turbulent boundary layers. Part II: Effect of wall temperature," *Journal of Fluid Mechanics*, Vol. 655, pp. 419–445.

[23]Ozawa, T., Wang, A., Modest, M. F., and Levin, D. A., "Particle Methods for Simulating Atomic Radiation in Hypersonic Reentry Flows," *Rarefied gas dynamics, Kyoto, Japan*, Vol. 1084, 2008.

[24]"CFD solution courtesy of NASA Ames," Vol. xxx, 2008, pp. xxx.

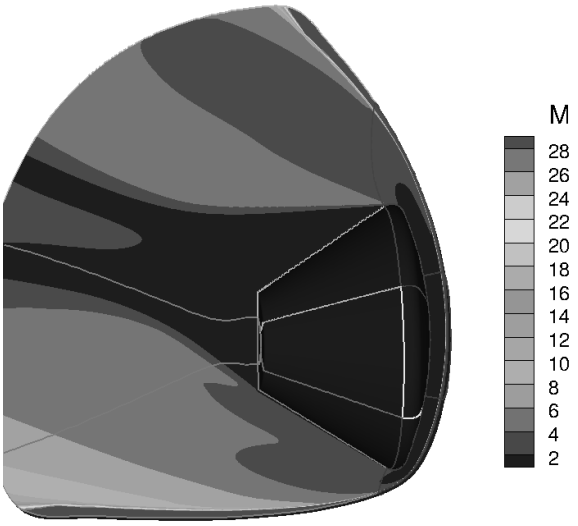


**Figure 1. Mach number contours for a three-dimensional DPLR solution of Orion at peak-heating reentry conditions.**[24]

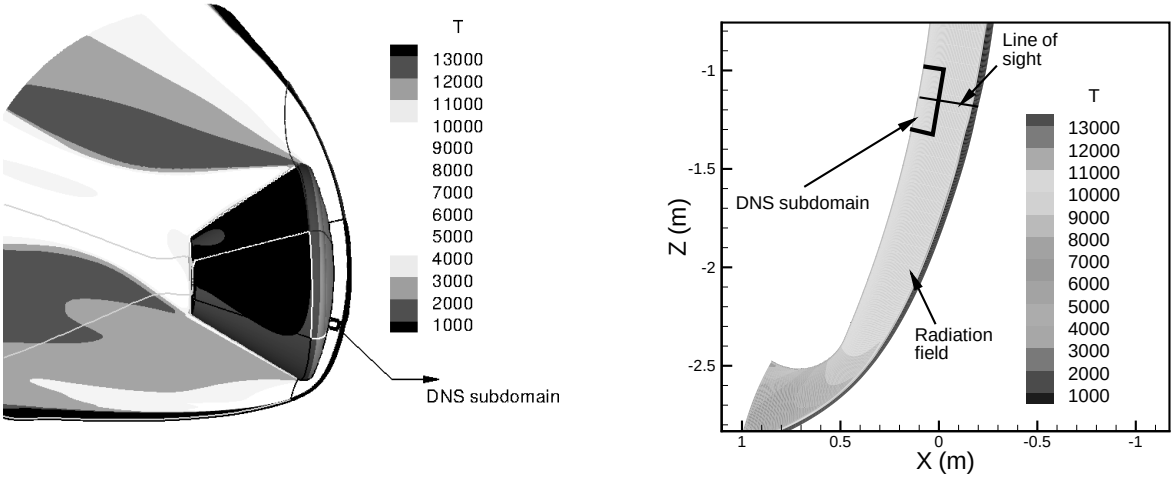


(a) (b)

**Figure 2. DNS subdomain from CEV solution.**

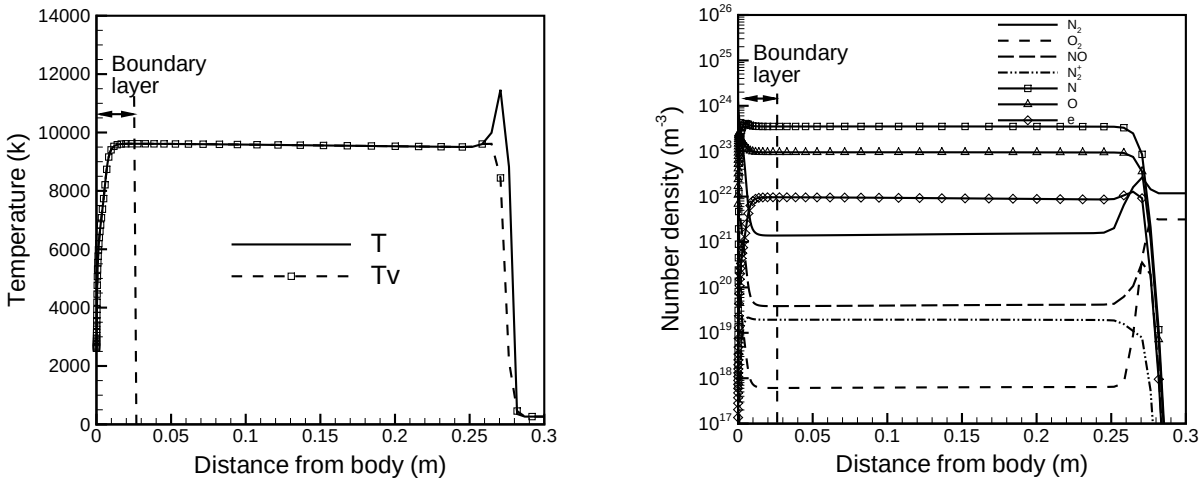


(a) (b)

**Figure 3. Temperatures and number densities along the line of sight indicated in Figure 2($b$) from the DPLR RANS solution.**

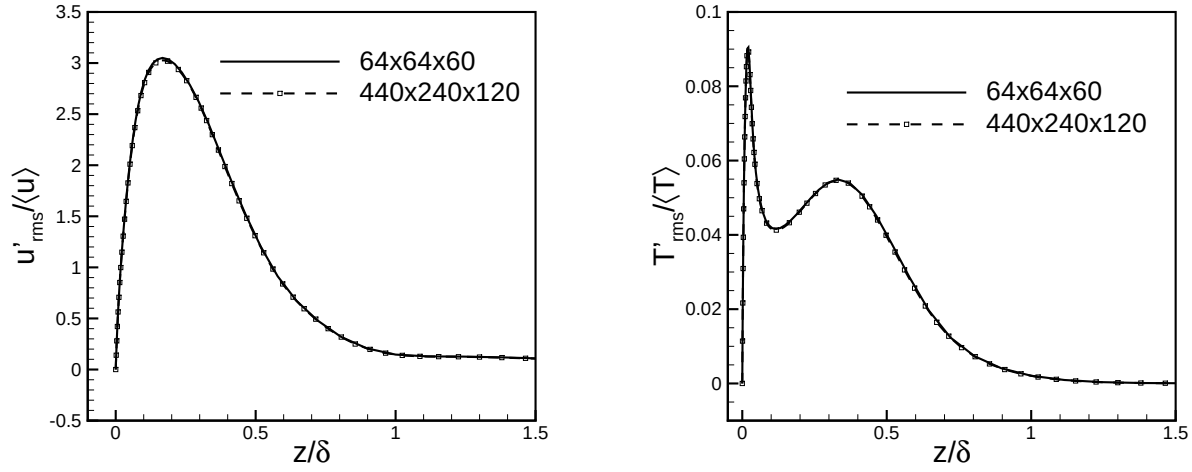


(a) (b)

**Figure 4. Grid convergence study varying $N_x \times N_y \times N_z$ for the DNS case without radiation coupling.**

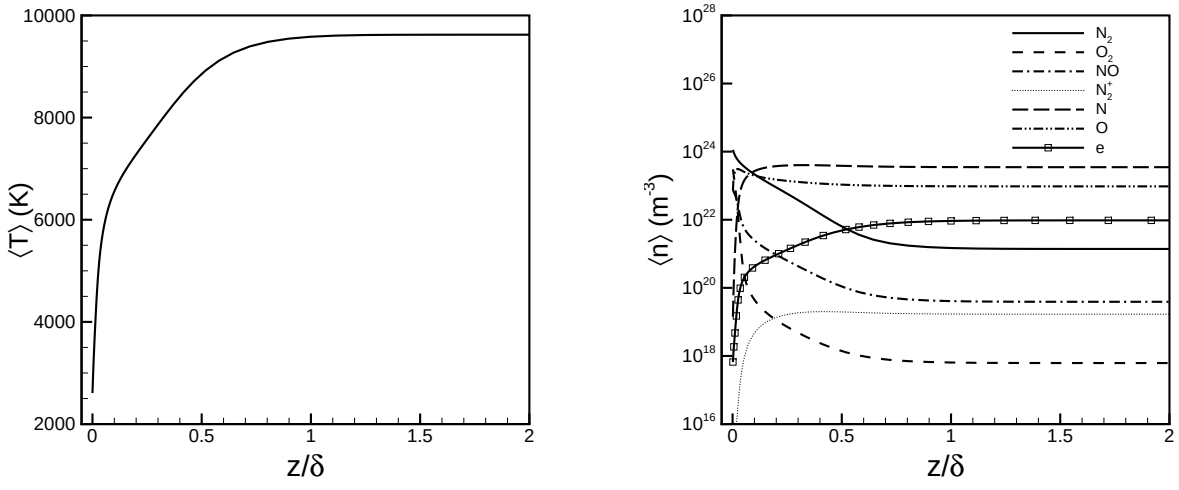


(a) (b)

**Figure 5. Mean temperature and species number densities for the DNS case without radiation coupling.**

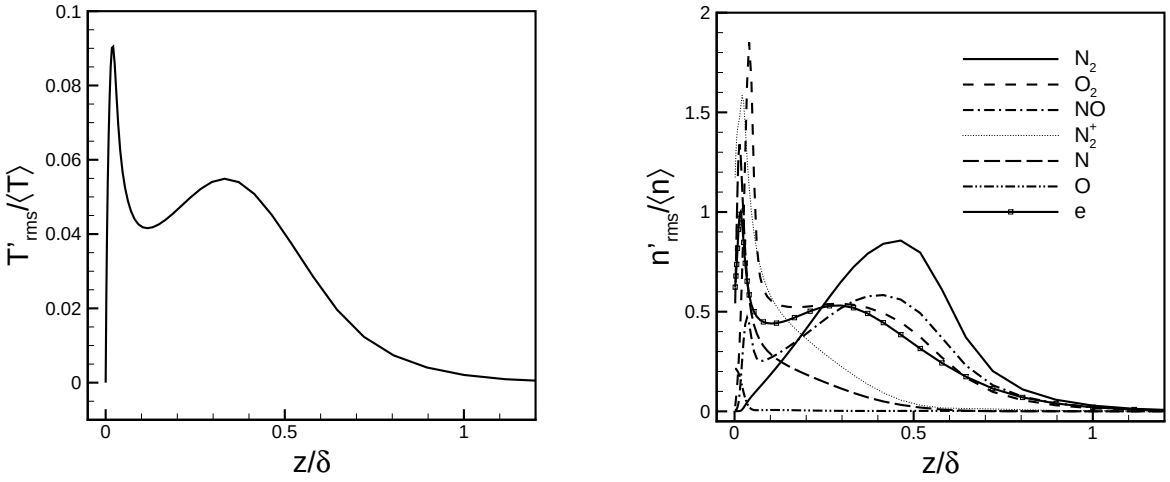


(a) (b)

**Figure 6. Fluctuations in temperature and species number densities relative to local mean for the DNS case without radiation coupling.**

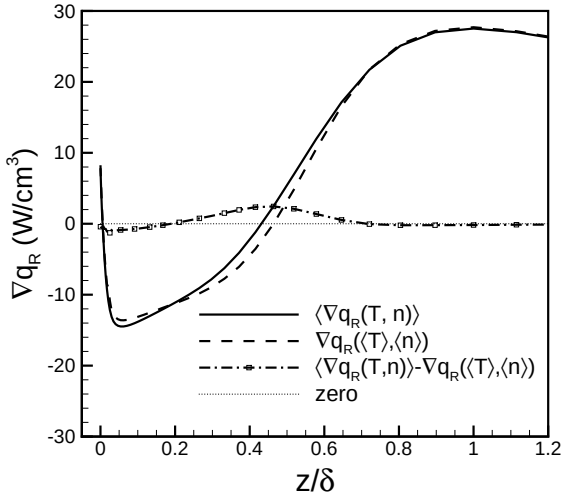


**Figure 7. 'Turbulent' and 'laminar' radiative source term $\nabla \cdot \mathbf{q}$ across the boundary layer for the DNS case without radiation coupling.**

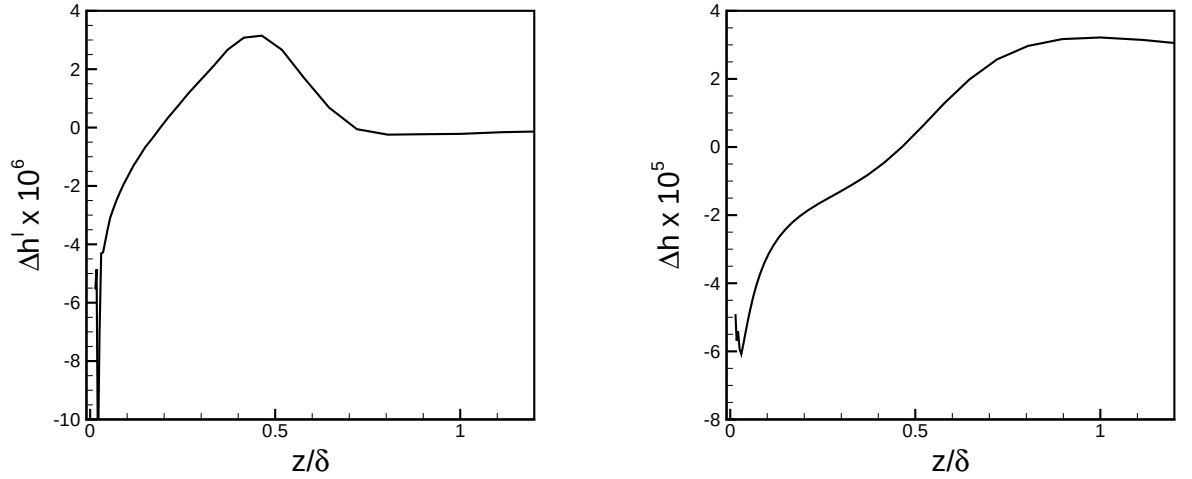


(a) (b)

**Figure 8. (*a*) 'Interaction' radiative heat ratio $\overline{\Delta h^I}$, defined by Equation 3 and (*b*) radiative heat ratio $\overline{\Delta h}$, defined by Equation 2 across the boundary layer for the DNS case without radiation coupling.**

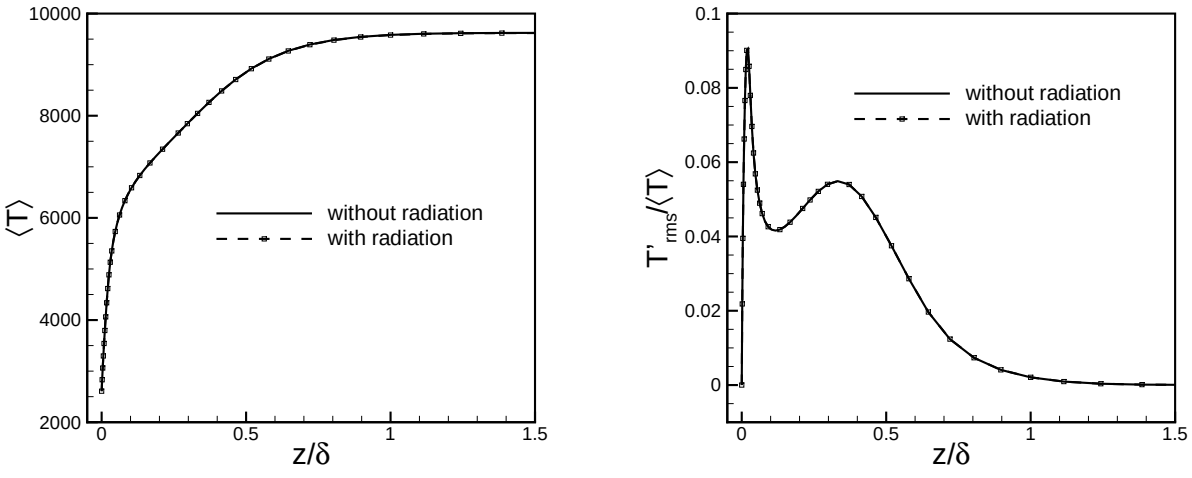


(a) (b)

**Figure 9. Mean and RMS of temperature for DNS cases with and without radiation coupling.**

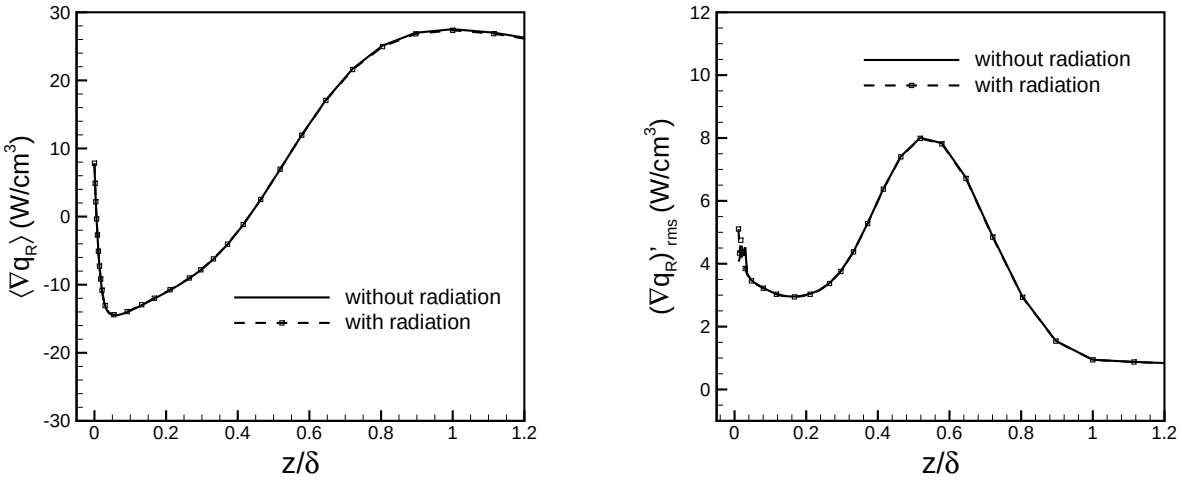


(a) (b)

**Figure 10. Mean and RMS of radiative source term for DNS cases with and without radiation coupling.**

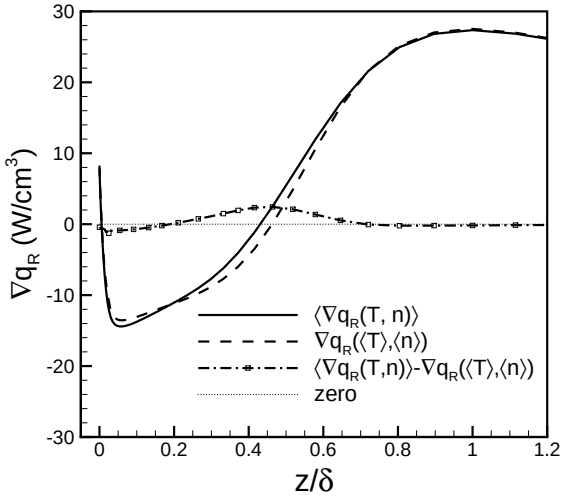


**Figure 11. 'Turbulent' and 'laminar' radiative source term $\nabla \cdot \mathbf{q}$ across the boundary layer for the DNS case with radiation coupling.**

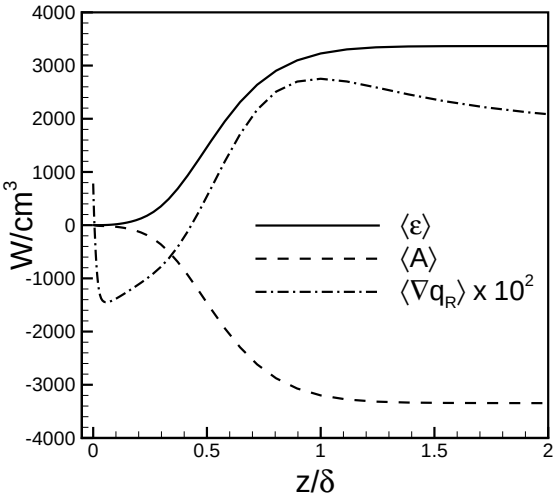


**Figure 12. Total emission $\bar{\varepsilon}$, absorption $\overline{A}$, and radiative source term $\overline{\nabla \cdot \mathbf{q}}$ across the boundary layer.**